applied sciences

MDPI

Article

Na-Doping Effects on Thermoelectric Properties of $Cu_{2-x}Se$ Nanoplates

Yingshi Jin, Mi-Kyung Han * and Sung-Jin Kim *

Department of Chemistry and Nano Science, Ewha Womans University, Seoul 120-750, Korea; allkdy77@gmail.com

* Correspondence: mikihan@ewha.ac.kr (M.-K.H.); sjkim@ewha.ac.kr (S.-J.K.); Tel.: +82-23-277-4164 (M.-K.H. & S.-J.K.)

Received: 23 November 2017; Accepted: 20 December 2017; Published: 22 December 2017

Abstract: For this work, a β-phase $Cu_{2-x}Se$ nanowire and nanoplate, and a Na-doped $Cu_{2-x}Se$ nanoplate were successfully synthesized using solution syntheses. The morphologies of the $Cu_{2-x}Se$ nanowire and nanoplate could be easily controlled by changing the synthetic condition. The Na-doped $Cu_{2-x}Se$ nanoplate was prepared by a simple treatment of the $Cu_{2-x}Se$ nanoplate with a sodium hydroxide-ethylene glycol solution. The nanopowders were then consolidated to bulk materials using spark plasma sintering (SPS). The phase structure and the microstructure of all of the samples were checked using X-ray diffraction (XRD), high-resolution transmission electron microscope (HR-TEM), and scanning electron microscope (SEM) analyses. The thermoelectric transport properties, such as the electrical conductivity, Seebeck coefficient, carrier concentration, carrier mobility, and thermal conductivity, were measured at temperature ranges from 323 to 673 K. The results show that Na played two important roles: one is reducing the carrier concentration, thereby improving the Seebeck coefficient, the other is reducing the thermal conductivity. Overall, the maximum thermoelectric figure of merit (ZT) of 0.24 was achieved at 673 K in the Na-doped $Cu_{2-x}Se$ nanoplate.

Keywords: $Cu_{2-x}Se$; doping; thermoelectric properties

1. Introduction

Thermoelectrics (TEs) is one of the most fascinating topics in the field of sustainable energy utilization due to its ability of direct conversion between electricity and heat based on either Seebeck or Peltier effects [1–3]. The efficiency of thermoelectric conversion is mostly dependent on the materials' dimensionless figure of merit (ZT) that is defined as $ZT = (S^2\sigma/\kappa_{tot})T$, where S is the Seebeck coefficient (or thermopower), σ is the electrical conductivity, κ_{tot} is the thermal conductivity ($\kappa_{tot} = \kappa_{elec.} + \kappa_{latt.}$, where $\kappa_{elec.}$ and $\kappa_{latt.}$ are the electronic and lattice contributions, respectively), and T is the temperature in Kelvin [4]. High-performance TE materials require a large Seebeck coefficient, low thermal conductivity, and high electrical conductivity. It is difficult, however, to concurrently improve all of the parameters because these three parameters are interrelated by carrier concentration. Recently, several strategies and concepts indicated that higher ZT values could be obtained in nanomaterials by a tailoring of the band structure and the phonon scattering [5–11]. Therefore, the pursuit of different TE materials using low-dimensional systems has recently become an active research field.

Recently, the copper chalcogenides $Cu_{2-x}Q$ (Q = S, Se, Te) have attracted great attention as a promising TE material due to not only their exceptional thermal- and electrical-transport properties, but also their unique features of being environmentally benign, earth-abundant composition, and low cost. Therefore, they can be a potential candidate as a medium-temperature thermoelectric material. $ZT > 2$ has been identified in these binary copper chalcogenides. (ZT values of 1.7–1.9 for $Cu_{2-x}S$ [12–18], 1.3–2.1 for $Cu_{2-x}Se$ [14–17], and 0.3–1.1 for $Cu_{2-x}Te$ [18–20]). Chemical doping

has been widely adopted to tune the carrier concentration and improve the ZT of thermoelectric materials [21–27].

Following this idea, in the present study, $Cu_{2-x}Se$ nanocrystals were successfully synthesized via an aqueous approach. The morphologies of $Cu_{2-x}Se$ can be tunable from plate to wire by changing synthetic conditions. A sodium doped $Cu_{2-x}Se$ nanoplate was prepared. After consolidating the nanopowders using spark plasma sintering (SPS), an evaluation of the thermoelectric properties was performed.

2. Materials and Methods

2.1. Materials

All of the reagents were used as received without further purification. Selenium powder (~100 mesh, 99.5%, Sigma Aldrich, St. Louis, MO, USA), sodium hydroxide (98%, Sam-Chun Pure Chemicals, Pyeongtaek, Korea), copper nitrate 3-hydrate (99~104%, Sigma Aldrich, USA), hydrazine hydrate (50~60%, Sigma Aldrich, USA), ethylene glycol (99.5%, Duksan Pure Chemicals, Ansan, Korea) and distilled water were used for the synthesis.

2.2. Synthesis of $Cu_{2-x}Se$ Nanoplate and Nanowire

$Cu_{2-x}Se$ was synthesized with different morphologies according to the method reported by Xu et al. with a slight modification [28]. For the synthesis of the $Cu_{2-x}Se$ nanoplate, 0.02 mol of Se powder, 1.25 mol of NaOH, and 8.00 mL $N_2H_4 \cdot H_2O$ were dissolved in 200 mL of distilled water. The solution was heated to 373 K and held there for 1 h to completely dissolve the selenium powder, thereby forming a clear deep red colored solution. Then, 15.39 mL of a 0.5 M $Cu(NO_3)_2$ aqueous solution was quickly added to the selenium precursor solution and kept for 30 min under this condition. The as-obtained product was washed with distilled water several times, and then dried under a vacuum at room temperature. For the $Cu_{2-x}Se$ nanowire, 0.02 mol of Se powder, 1.25 mol of NaOH, and 8.00 mL of $N_2H_4 \cdot H_2O$ was dissolved in 50 mL of distilled water, and followed the same procedure used in the case of $Cu_{2-x}Se$ nanoplates except heating the solution for 1 h at 373 K after injecting the Cu source.

2.3. Synthesis of Na-Doped $Cu_{2-x}Se$ Nanoplate

Sodium was incorporated via the following step: the as-synthesized $Cu_{2-x}Se$ nanoplate (2.6 g) were reacted with sodium hydroxide-ethylene glycol solution (3.1 M) under vigorous stirring at 413 K for 24 h. Finally, the products were collected by centrifugation after a number of washing procedures with acetone and ethanol.

2.4. Characterization of Materials

The synthesized samples were characterized using powder X-ray diffraction (PXRD), scanning electron microscope (SEM), high-resolution transmission electron microscope (HR-TEM), and inductively coupled plasma-optical emission spectroscope (ICP-OES) analyses. The PXRD patterns were obtained with a Rigaku powder X-ray Diffractometer (Rigaku Co., Shibuya-Ku, Tokyo, Japan) using Cu-K_α radiation (λ = 1.5418 Å) at 40 kV and 30 mA with the 2θ range from 20° to 80°. The diffraction data were collected at a scanning rate of 2 °/min. The SEM images were investigated using a JEOL JSM-6700F (JEOL Ltd., Tokyo, Japan) at an accelerating voltage of 10 kV. The TEM images, selected area electron diffraction (SAED) pattern and energy-dispersive X-ray spectroscopy mapping (EDS-mapping) were recorded on a JEOL JEM-2100F instrument (JEOL Ltd., Tokyo, Japan). The chemical compositions were collected by ICP-OES using an OPTIMA 8300 (PerkinElmer, Inc., Waltham, MA, USA).

2.5. Characterization of the Thermoelectric Properties

In order to measure thermoelectric properties, pellets with a diameter of ~10 mm and a thickness of ~2 mm were fabricated using the spark plasma sintering (SPS-211lx, Fuji Electronic Industrial Co.,

Ltd., Osaka, Japan). Typically, ~2 g of the powder was loaded in a graphite die with an inner diameter of 10 mm. The powder was heated to the 450 °C at a heating rate of 100 °C/min under the conditions of vacuum and at a uniaxial pressure of ~50 MPa, and the holding time was 5 min at the sintering temperature. The electrical conductivity and the Seebeck coefficient were measured under a low-pressure helium atmosphere using ZEM-3 equipment (Ulvac-Riko, ULVAC Inc., Yokohama, Kanagawa, Japan). Thermal conductivity was determined by combining thermal diffusivity (D), specific heat (C_p) and sample density (ρ) according to $\kappa_{tot} = D \times C_p \times \rho$. The thermal diffusivity (D) and specific heat (C_p) of the samples were measured using a NETZSCH LFA 457 MicroFlash™ instrument (NETZSCH, Selb, Germany) under a vacuum atmosphere. The ρ was measured using the sample's geometry and mass. Generally, the uncertainties of the electrical conductivity, Seebeck coefficient, and thermal conductivity are estimated to be approximately 7%, 5% and 7%, respectively. The uncertainty of ZT is to be about 20%. The Hall resistivity was measured using a physical property measurement system (PPMS Dynacool-14T, Quantum Design, San Diego, CA, USA).

3. Results and Discussion

The XRD patterns of the as-synthesized samples of undoped $Cu_{2-x}Se$ nanowire and nanoplate and Na-doped $Cu_{2-x}Se$ nanoplate are shown in Figure 1. All of the reflection peaks can be indexed to the face-centered-cubic $Cu_{1.8}Se$ (JCPDS 71-0044), and no impurities were detected within the detection limit of the X-ray. The peaks for $Cu_{2-x}Se$ nanowire sample are quite broad mainly due to the finite size of our products. The lattice constants can be refined as a = 5.674 (1), 5.737 (1) and 5.738 (1) Å for nanowire, nanoplate and Na-doped nanoplate $Cu_{2-x}Se$ samples, respectively, which match the literature value listed on JCPDS Card No. 71-0044 well. It can be concluded that the lattice constant of the as-synthesized nanopowders is unchanged upon Na doping. This implies that Cu^+ (0.077 nm) ions are not substituted by much larger Na^+ (0.133 nm) ions in this experimental condition. A similar result was observed when Na was doped in a system of Cu_9S_5 [29]. On the other hand, Na-doped $Cu_{2-x}Se$ shows a peak shift in comparison with the pattern of as-synthesized Na-doped $Cu_{2-x}Se$ nanoplates after the SPS process (refer to the inset 002 peaks). The lattice constants for Na-doped nanoplate $Cu_{2-x}Se$ samples after SPS is 5.766 (9) Å. This small lattice expansion (~5%) may be the result of Na incorporation into the structure of $Cu_{2-x}Se$ by electrochemical reactions at the interfaces during the SPS process. Rather than the shift peak position, the SPS process did not significantly modify the crystal structure of nanoplate and Na-doped nanoplate sample. However, the structural changes occur for nanowire samples from cubic to orthorhombic $Cu_{2-x}Se$ after SPS treatment, although they were sintered under the same conditions (i.e., 450 °C, 50 MPa, and 5 min) by the SPS technique.

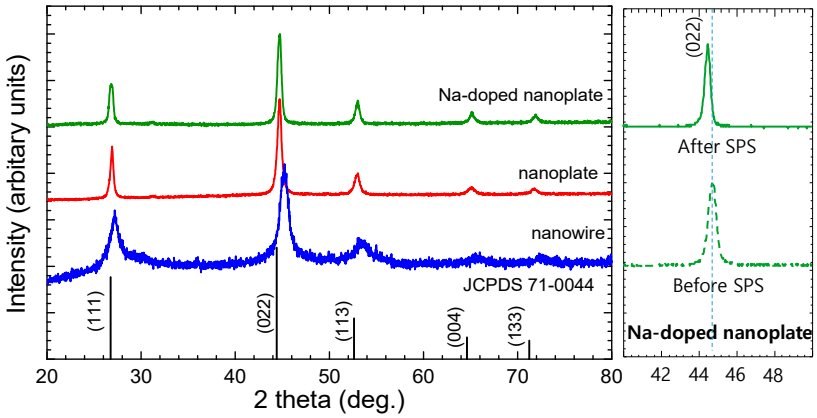

Figure 1. Powder X-ray diffraction (XRD) patterns of as-synthesized samples of nanowire, nanoplate and Na-doped nanoplate $Cu_{2-x}Se$ compared with those of the standard cards (JCPDS 71-0044). The inset shows the comparison of peak position for as-synthesized (dashed line) and after SPSed (solid line) samples of Na-doped $Cu_{2-x}Se$ nanoplate. (SPS: spark plasma sintering)

According to the Hall coefficient measurements, the carrier concentrations of nanoplate and Na-doped nanoplate are estimated to be $5.71 \times 10^{22}/cm^3$ and $2.80 \times 10^{22}/cm^3$, respectively. Na doping reduce the carrier concentration of $Cu_{2-x}Se$. This means that Na acts as an electron donor to the nanoplate. The generated electrons by Na recombine with holes, resulting in a decrease of the hole concentration by the electron–hole pairs [30]. This is consistent with the observed decreased electrical conductivity in Na-doped $Cu_{2-x}Se$ nanoplates shown in the next section. As expected, Na-doped nanoplate showed a lower carrier mobility than an undoped nanoplate due to the higher carrier concentration. The carrier mobility of nanoplate and Na-doped nanoplate were estimated to be 0.96 and 1.32 cm^2/Vs, respectively.

In our synthetic process, $Cu_{2-x}Se$ with different shapes were achieved under different conditions (see Experimental Section for details). Figure 2 shows the morphologies of the as-obtained $Cu_{2-x}Se$ observed by SEM. It was found that the morphology of products depends on the concentration of reactants and the reducing reagent. It is not very clearly known at present why reaction concentration can change the morphologies significantly. One possible reason may be that the concentration affects the growth rate of crystals [31]. Figure 2a,b display the SEM images of the $Cu_{2-x}Se$ nanoplate with a hexagonal morphology. In general, the lateral dimensions of the nanoplates are 1–3 μm. The thickness of the nanoplate was about ~50 nm, shown in a vertical SEM image of a single $Cu_{2-x}Se$ nanoplate (Figure 2b). Figure 2c,d show SEM images of $Cu_{2-x}Se$ nanowire with lengths larger than ~30 μm and diameters of ~200 nm.

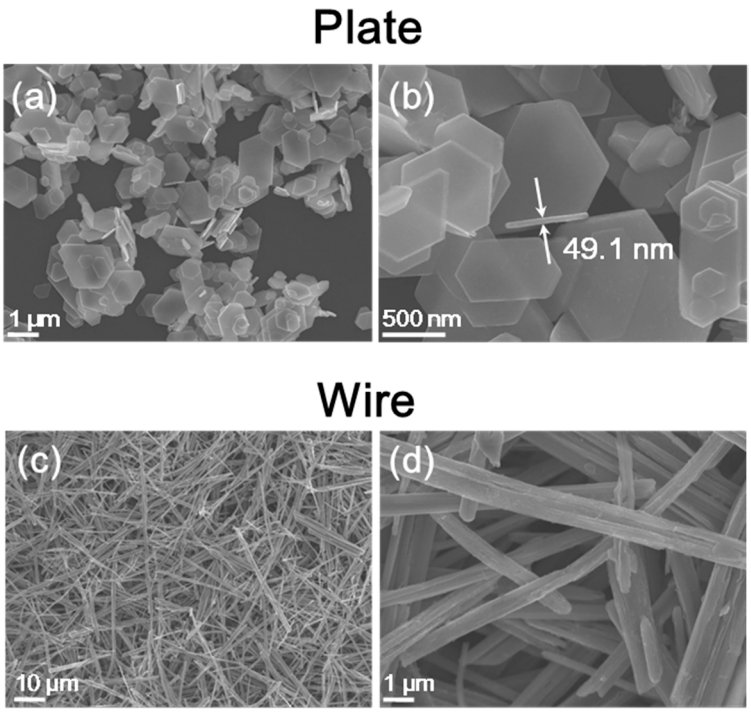

Figure 2. Scanning electron microscope (SEM) images of (**a**,**b**) nanoplate; and (**c**,**d**) nanowire of $Cu_{2-x}Se$ powder.

Figure 3a shows the SEM images of Na-doped $Cu_{2-x}Se$ nanoplates. The size and shape of Na-doped nanoplate are similar to those of undoped $Cu_{2-x}Se$ nanoplate. The TEM image of a typical Na-doped $Cu_{2-x}Se$ nanoplate is shown in Figure 3b, where a hexagonal shaped nanoplate can be clearly identified. The inset of Figure 3b is a selected-area electron diffraction pattern taken along the [111] direction of the nanoplate, showing the single crystallinity of the nanoplate. To check the chemical composition of the $Cu_{2-x}Se$ samples, energy-dispersive spectroscopy (EDS) and inductively coupled plasma optical emission spectroscopy (ICP-OES) are performed. The result of elemental-mapping

using the TEM-EDS analysis is shown in Figure 3c. The distributions of the elements Cu, Se, and Na are homogeneous in Na-doped $Cu_{2-x}Se$ nanoplate. About ~16% of Na was detected in Na-doped $Cu_{2-x}Se$ nanoplate. Similar results were observed by inductively coupled plasma optical emission spectroscopy (ICP-OES), shown in Table 1. The atomic ratio of Cu and Se for $Cu_{2-x}Se$ nanoplate calculated from the ICP-OES results is around 63.7:36.3, whereas the Na-doped $Cu_{2-x}Se$ nanoplate has atomic ratio between Cu:Se of around 63.6:31.3, which means that the Na-doped $Cu_{2-x}Se$ nanoplate we got through the two-step procedure is the Cu-rich $Cu_{2-x}Se$ phase.

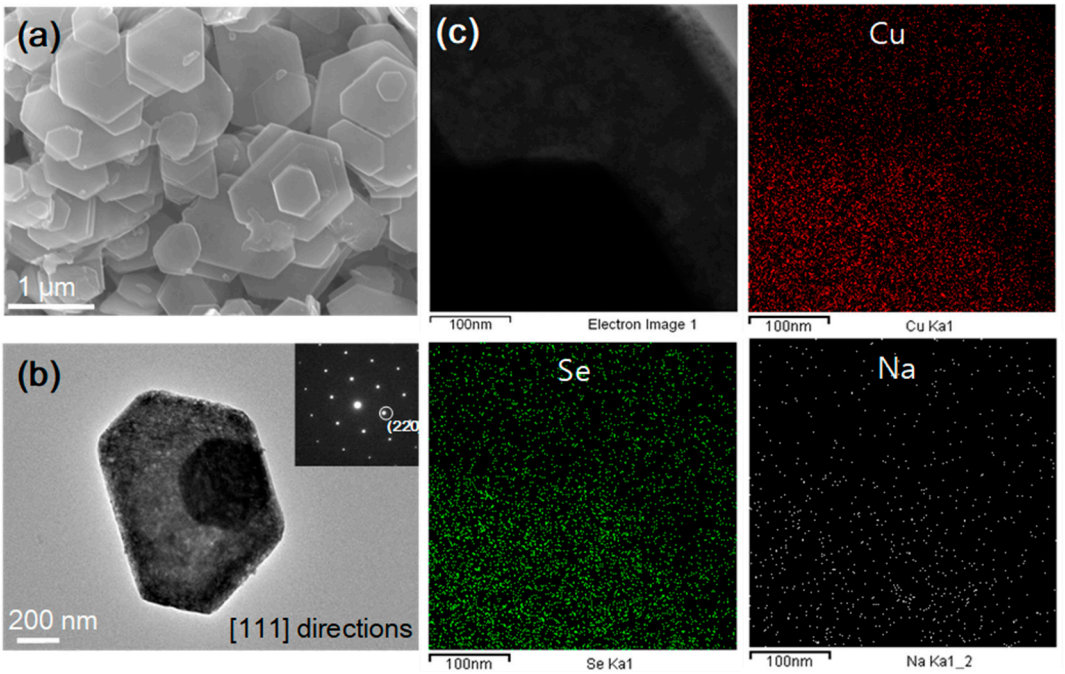

Figure 3. (**a**) SEM image; (**b**) Transmission electron microscope (TEM) image with selected area electron diffraction (SAED) patterns (inset) for Na-doped $Cu_{2-x}Se$ nanoplates; (**c**) the corresponding mapping on compositions by an energy-dispersive spectrometer (EDS) for Na-doped $Cu_{2-x}Se$ nanoplate.

Table 1. Atomic ratio of Cu, Se, and Na for $Cu_{2-x}Se$ calculated from ICP-AES.

Sample	Na	Cu	Se	Composition
$Cu_{2-x}Se$-wire	-	0.613	0.397	$Cu_{1.59}Se$
$Cu_{2-x}Se$-plate	-	0.637	0.363	$Cu_{1.75}Se$
Na-$Cu_{2-x}Se$-plate	0.051	0.636	0.313	$Na_{0.162}Cu_{2.03}Se$

The SPS pressed Na-doped $Cu_{2-x}Se$ bulk sample was also characterized by X-ray photoelectron spectroscopy (XPS). The XPS spectra provide useful information for understanding the chemical bonding states of the constituent atoms. The binding energies obtained in the XPS analysis were corrected for specimen charging by a setting C 1s to 284.6 eV. Representative XPS spectra of Na, Cu, and Se are shown in Figure 4. As shown in Figure 4b, one strong peak located at 1071.7 eV, indicative of Na 1s, suggested the existence of Na^+ species in Na-doped $Cu_{2-x}Se$ nanoplates. As shown in Figure 4c,d, the resulted binding energies of Se 3d and Cu $2p_{3/2}$ are given as 54.0 and 933.4 eV, respectively. All of the observed binding energy values for Cu 2p and Se 3d are nearly in agreement with the reported data in the literature [30]. In the literature, the binding energy of Cu $2p_{3/2}$ has been reported to be ~933 eV regardless of its oxidation state (Cu^0, Cu^{1+} and Cu^{2+}) [31,32]. Generally, Cu^{2+} is best distinguished from other Cu oxidation states by observing low-intensity satellite peaks in the region of 940–950 eV. According to Figure 4c, the satellite peaks indicate that the presence of

Cu^{2+} ion in bulk Na-doped $Cu_{2-x}Se$ nanoplates. A significant broadening of the Se 3d spectra is observed, as shown in Figure 4d. Similar features were previously found in InSe compounds upon Na deposition [33].

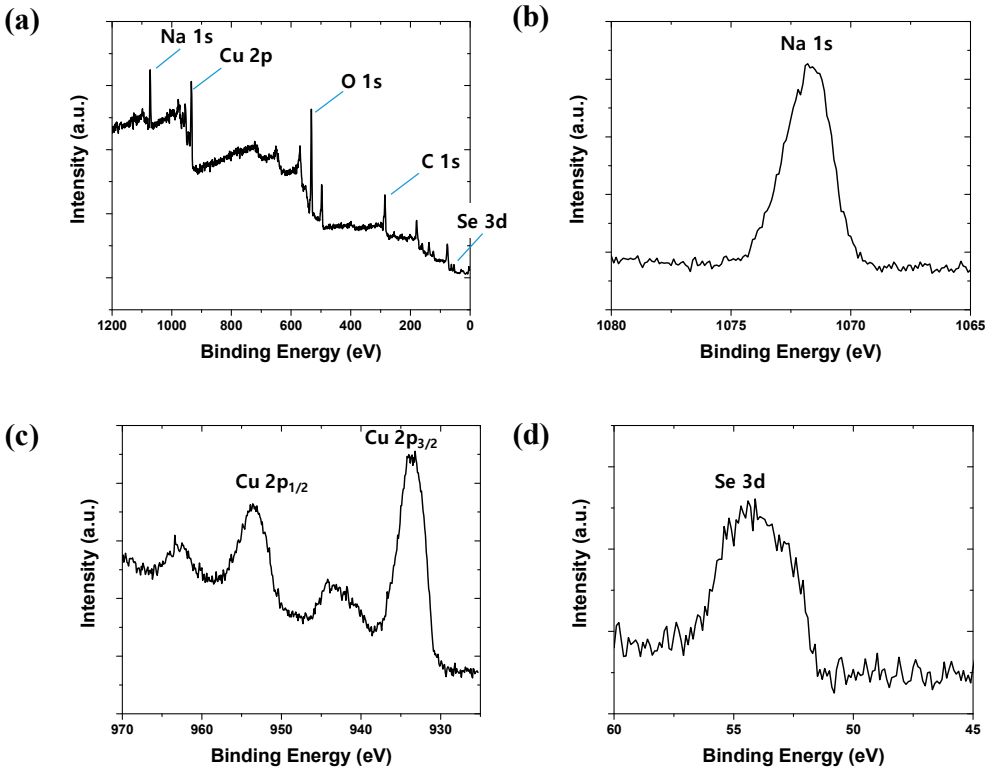

Figure 4. (**a**) X-ray photoelectron spectroscopy (XPS) survey spectra, and high-resolution XPS spectra of (**b**) Na; (**c**) Cu; and (**d**) Se ions of SPSed Na-doped $Cu_{2-x}Se$ sample.

Figure 5 shows the electrical and thermal properties of SPSed bulk pellets of nanowire, nanoplate, and Na-doped $Cu_{2-x}Se$ nanoplate, and compared to that of bulk $Cu_{1.75}Se$ sample [32]. For all of the samples, with the increase of the temperature, the electrical conductivity decreases, indicating a degenerated semiconductor behavior, shown in Figure 5a. The electrical conductivity of SPSed bulk pellets of nanowire is relatively lower than those of the other two samples, which is mainly due to the presence of point defects and dislocations by Cu vacancies in the pellet along with lower symmetry. Compared to the bulk, the undoped $Cu_{2-x}Se$ nanoplates exhibited a similar electrical conductivity. It is observed that a Na doped $Cu_{2-x}Se$ nanoplate sample shows lower electrical conductivity than a $Cu_{2-x}Se$ nanoplate sample. The reason for this may be the reduction of the carrier concentration by Na-doping.

Figure 5b shows the temperature dependences of the Seebeck coefficients. All samples possess a positive Seebeck coefficient in the measured temperature range. This means that the $Cu_{2-x}Se$ samples exhibit p-type conduction and the majority carriers are holes, which is consistent with the Hall measurements. It can be seen that the Seebeck coefficients increase from 10 to 70 μV/K with increasing temperature. It is observed that Na doped $Cu_{2-x}Se$ nanoplate sample shows a slightly higher Seebeck coefficient than that of the undoped $Cu_{2-x}Se$ nanoplate sample. This result can be attributed to the lower carrier concentration by Na doping.

Based on the results of the electrical conductivity and the Seebeck coefficient, the power factor (*PF*) of all of the samples can be calculated according to the equation $PF = \sigma S^2$. As shown in Figure 5c, the power factor increases as temperature increases due to the increased values of Seebeck coefficients. Because of a high electrical conductivity, the maximum power factor of the undoped $Cu_{2-x}Se$ nanoplate

is 6.5 μW/cmK^2 (at ~673 K). A Na-doped $Cu_{2-x}Se$ nanoplate has a slightly lower PF when compared to the $Cu_{2-x}Se$ nanoplate. The peak PF values of 3.9 μW/cmK^2 (at ~673 K) was observed for the Na-doped $Cu_{2-x}Se$ nanoplate. This lower PF is mainly owing to the lower electrical conductivity of Na-doped $Cu_{2-x}Se$ nanoplate samples.

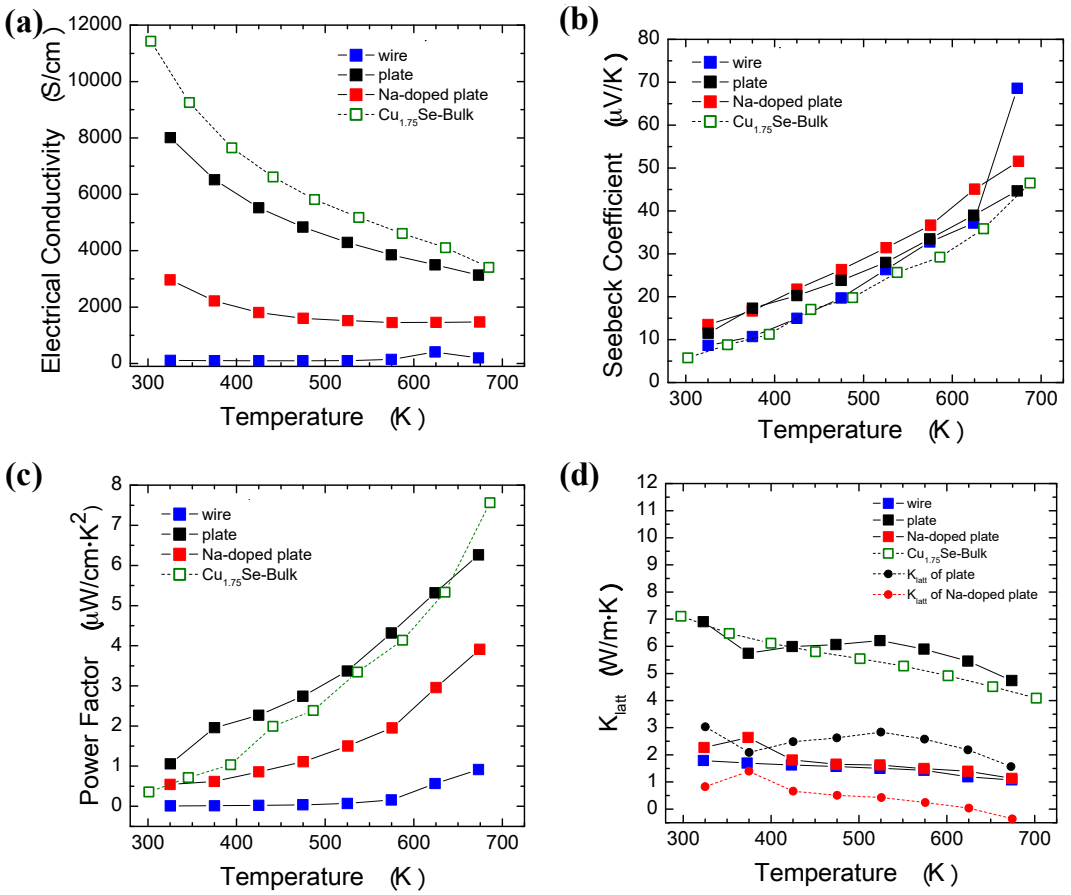

Figure 5. Temperature dependent thermoelectric properties of nanowire, nanoplate and Na-doped nanoplate $Cu_{2-x}Se$ samples: (**a**) electrical conductivity; (**b**) Seebeck coefficient; (**c**) Power factor; (**d**) thermal conductivity along with the lattice contribution to the thermal conductivities. Solid dots are experimental data in this work, while open dots are bulk $Cu_{1.75}Se$ samples from reference [34].

As shown in Figure 5d, the thermal conductivity of all of the samples decreased gradually with increasing temperature. Owing to the α–β phase transition in $Cu_{2-x}Se$ compounds, an anomalous behavior of thermal conductivity is observed near 373 K [35]. The thermal conductivities of the Na-doped $Cu_{2-x}Se$ samples are lower than that of the undoped $Cu_{2-x}Se$ nanoplate sample. The total thermal conductivity (κ_{tot}) is the sum of two contributions, one from the charge carriers ($\kappa_{elec.}$), and the other from the lattice vibrations ($\kappa_{latt.}$), ($\kappa_{tot} = \kappa_{elec.} + \kappa_{latt.}$). Here $\kappa_{elec.}$ is estimated by the Wiedemann–Franz relationship, $\kappa_{elec.} = L_0\sigma T$, where L_0 is the Lorenz number, σ is the electrical conductivity and T the absolute temperature. The value of Lorenz number ($L_0 = 1.5 \times 10^{-8}$ WΩ/K^2) [35] for $Cu_{2-x}Se$ is used to estimate κ_{elec}.. The $\kappa_{latt.}$ values are calculated by subtracting $\kappa_{elec.}$ from κ_{tot}, present in Figure 5d. The $\kappa_{latt.}$ values of undoped and Na-doped $Cu_{2-x}Se$ at 300 K are ~3.03 W/m·K and ~0.83 W/m·K, respectively. Regardless of the exact mechanism, Na appears to play a role in lowering the lattice thermal conductivity.

According to the above measured results of electrical conductivity, the Seebeck coefficient and the thermal conductivity, the dimensionless figure of merit ZT can be calculated using the formula $ZT = S^2\sigma T/\kappa$, as shown in Figure 6. It can be seen that the ZT values of all of the samples were

increased with the increasing temperature. Benefiting from the carrier concentration optimization and low thermal conductivity, the Na-doped $Cu_{2-x}Se$ shows the highest *ZT* value among all of the samples over the entire temperature range. The maximum *ZT* value of 0.24 was obtained at 673 K for a Na-doped $Cu_{2-x}Se$ sample, which is greater than those of undoped $Cu_{2-x}Se$ nanowire and nanoplate. It indicates that Na doping can indeed increase the figure of merit of the $Cu_{2-x}Se$ nanoplates.

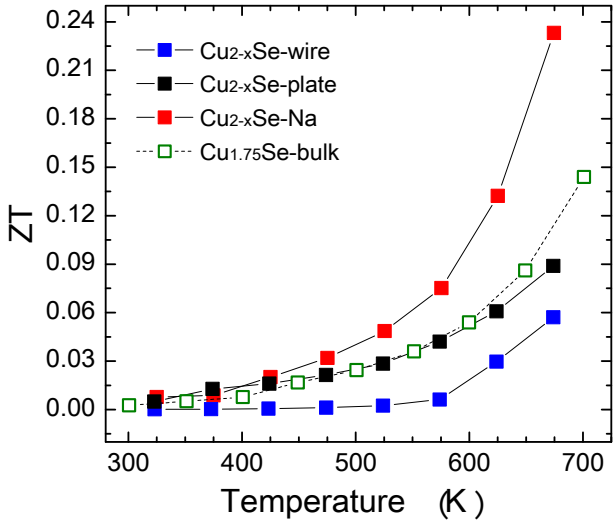

Figure 6. Temperature-dependent dimensionless figure of merit (*ZT*) for nanowire, nanoplate and Na-doped $Cu_{2-x}Se$ nanoplate samples along with the data for bulk $Cu_{1.75}Se$ samples from reference [34].

4. Conclusions

In conclusion, surfactant-free $Cu_{2-x}Se$ nanowires and nanoplates have been successfully synthesized by an aqueous approach, and a Na-doped $Cu_{2-x}Se$ nanoplate was prepared by heat treatment of $Cu_{2-x}Se$ nanoplates in a sodium hydroxide-ethylene glycol solution at 413 K for 24 h. The decreasing carrier concentrations and electrical conductivities upon Na-doping indicate that sodium cations act as an n-type dopant, which is a key for increasing Seebeck coefficient and decreasing electronic thermal conductivity. The *ZT* value of 0.24 was obtained at 673 K from Na-doped $Cu_{2-x}Se$ nanoplate, which is much higher than that of undoped $Cu_{2-x}Se$ nanoplate (*ZT* ~0.09 at 673 K). This study provides a strategy for improvement of the thermoelectric performances.

Acknowledgments: This research was supported by the National Research Foundation of Korea (NRF) Grant funded by the Korean Government (MSIP) (NRF-2015R1A5A1036133).

Author Contributions: All authors participated in the research, data analysis and edition of the manuscript. Mi-Kyung Han and Sung-Jin Kim conceived and designed the experiments; Yingshi Jin performed the experiments; Mi-Kyung Han analyzed the data and wrote the paper.

Conflicts of Interest: The authors declare no conflicts of interest.

References

1. Snyder, G.J.; Toberer, E.S. Complex thermoelectric materials. *Nat. Mater.* **2008**, *7*, 105–114. [CrossRef] [PubMed]
2. Rowe, D.M. *CRC Handbook of Thermoelectrics*; CRC Press: New York, NY, USA, 1995.
3. Yang, L.; Chen, Z.-G.; Dargusch, M.S.; Zou, J. High performance thermoelectric materials: Progress and their applications. *Adv. Energy Mater.* **2017**, 1701797. [CrossRef]
4. Bell, L.E. Cooling, heating, generating power, and recovering waste heat with thermoelectric systems. *Science* **2008**, *321*, 1457–1461. [CrossRef] [PubMed]

5. Moshwan, R.; Yang, L.; Zou, J.; Chen, Z.-G. Eco-friendly SnTe thermoelectric materials: Progress and future challenges. *Adv. Funct. Mater.* **2017**, *27*. [CrossRef]
6. Zhang, Q.; Liao, B.L.; Lan, Y.C.; Lukas, K.; Liu, W.S.; Esfarjani, K.; Opeil, C.; Broido, D.; Chen, G.; Ren, Z.F. High thermoelectric performance by resonant dopant indium in nanostructured SnTe. *Proc. Natl. Acad. Sci. USA* **2013**, *110*, 13261–13266. [CrossRef] [PubMed]
7. Liu, W.; Tan, X.J.; Yin, K.; Liu, H.J.; Tang, X.F.; Shi, J.; Zhang, Q.J.; Uher, C. Convergence of Conduction Bands as a Means of Enhancing Thermoelectric Performance of n-Type $Mg_2Si_{1-x}Sn_x$ Solid Solutions. *Phys. Rev. Lett.* **2012**, *108*. [CrossRef] [PubMed]
8. Wang, H.; Gibbs, Z.M.; Takagiwa, Y.; Snyder, G.J. Tuning bands of PbSe for better thermoelectric efficiency. *Energy Environ. Sci.* **2014**, *7*, 804–811. [CrossRef]
9. Girard, S.N.; He, J.Q.; Zhou, X.Y.; Shoemaker, D.; Jaworski, C.M.; Uher, C.; Dravid, V.P.; Heremans, J.P.; Kanatzidis, M.G. High Performance Na-doped PbTe-PbS Thermoelectric Materials: Electronic Density of States Modification and Shape-Controlled Nanostructures. *J. Am. Chem. Soc.* **2011**, *133*, 16588–16597. [CrossRef] [PubMed]
10. Rhyee, J.S.; Lee, K.H.; Lee, S.M.; Cho, E.; Kim, S.I.; Lee, E.; Kwon, Y.S.; Shim, J.H.; Kotliar, G. Peierls distortion as a route to high thermoelectric performance in In_4Se_3-delta crystals. *Nature* **2009**, *459*, 965–968. [CrossRef] [PubMed]
11. Chen, Z.-G.; Han, G.; Yang, L.; Cheng, L.; Zou, J. Nanostructured thermoelectric materials: Current research and future challenge. *Prog. Nat. Sci.* **2012**, *22*, 535–549. [CrossRef]
12. He, Y.; Day, T.; Zhang, T.S.; Liu, H.L.; Shi, X.; Chen, L.D.; Snyder, G.J. High thermoelectric performance in non-toxic earth-abundant copper sulfide. *Adv. Mater.* **2014**, *26*, 3974–3978. [CrossRef] [PubMed]
13. Zhao, L.L.; Wang, X.L.; Fei, F.Y.; Wang, J.Y.; Cheng, Z.X.; Dou, S.X.; Wang, J.; Snyder, G.J. High thermoelectric and mechanical performance in highly dense $Cu_{2-x}S$ bulks prepared by a melt-solidification technique. *J. Mater. Chem. A* **2015**, *3*, 9432–9437. [CrossRef]
14. Zhao, K.P.; Blichfeld, A.B.; Chen, H.Y.; Song, Q.F.; Zhang, T.S.; Zhu, C.X.; Ren, D.D.; Hanus, R.; Qiu, P.F.; Iversen, B.B.; et al. Enhanced thermoelectric performance through tuning bonding energy in $Cu_2Se_{1-x}S_x$ liquid-like materials. *Chem. Mater.* **2017**, *29*, 6367–6377. [CrossRef]
15. Yang, L.; Chen, Z.G.; Han, G.; Hong, M.; Zou, Y.C.; Zou, J. High-performance thermoelectric Cu_2Se nanoplates through nanostructure engineering. *Nano Energy* **2015**, *16*, 367–374. [CrossRef]
16. Gahtori, B.; Bathula, S.; Tyagi, K.; Jayasimhadri, M.; Srivastava, A.K.; Singh, S.; Budhani, R.C.; Dhar, A. Giant enhancement in thermoelectric performance of copper selenide by incorporation of different nanoscale dimensional defect features. *Nano Energy* **2015**, *13*, 36–46. [CrossRef]
17. Yang, L.; Chen, Z.-G.; Han, G.; Hong, M.; Zou, J. Impacts of Cu deficiency on the thermoelectric properties of $Cu_{2-x}Se$ nanoplates. *Acta Mater.* **2016**, *113*, 140–146. [CrossRef]
18. He, Y.; Zhang, T.S.; Shi, X.; Wei, S.H.; Chen, L.D. High thermoelectric performance in copper telluride. *NPG Asia Mater.* **2015**, *7*, e210. [CrossRef]
19. Mallick, M.M.; Vitta, S. Realizing high figure-of-merit in Cu_2Te using a combination of doping, hierarchical structure, and simple processing. *J. Appl. Phys.* **2017**, *122*. [CrossRef]
20. Kurosaki, K.; Goto, K.; Kosuga, A.; Muta, H.; Yamanaka, S. Thermoelectric and thermophysical characteristics of Cu_2Te-Tl_2Te pseudo binary system. *Mater. Trans.* **2006**, *47*, 1432–1435. [CrossRef]
21. Ballikaya, S.; Chi, H.; Salvador, J.R.; Uher, C. Thermoelectric properties of Ag-doped Cu_2Se and Cu_2Te. *J. Mater. Chem. A* **2013**, *1*, 12478–12484. [CrossRef]
22. Zhao, L.L.; Wang, X.L.; Yun, F.F.; Wang, J.Y.; Cheng, Z.X.; Dou, S.X.; Wang, J.; Snyder, G.J. The effects of Te^{2-} and I^- substitutions on the electronic structures, thermoelectric performance, and hardness in melt-quenched highly dense $Cu_{2-x}Se$. *Adv. Electron. Mater.* **2015**, *1*. [CrossRef]
23. Yang, L.; Chen, Z.-G.; Han, G.; Hong, M.; Huang, L.; Zou, J. Te-doped Cu_2Se nanoplates with a high average thermoelectric figure of merit. *J. Mater. Chem. A* **2016**, *4*, 9213–9219. [CrossRef]
24. Liu, H.L.; Yuan, X.; Lu, P.; Shi, X.; Xu, F.F.; He, Y.; Tang, Y.S.; Bai, S.Q.; Zhang, W.Q.; Chen, L.D.; et al. Ultrahigh thermoelectric performance by electron and phonon critical scattering in $Cu_2Se_{1-x}I_x$. *Adv. Mater.* **2013**, *25*, 6607–6612. [CrossRef] [PubMed]
25. Balapanov, M.K.; Ishembetov, R.K.; Kuterbekov, K.A.; Kubenova, M.M.; Almukhametov, R.F.; Yakshibaev, R.A. Transport phenomena in superionic $Na_xCu_{2-x}S$ (x = 0.05; 0.1; 0.15; 0.2) compounds. *Ionics* **2017**. [CrossRef]

26. Olvera, A.A.; Moroz, N.A.; Sahoo, P.; Ren, P.; Bailey, T.P.; Page, A.A.; Uher, C.; Poudeu, P.F.P. Partial indium solubility induces chemical stability and colossal thermoelectric figure of merit in Cu_2Se. *Energy Environ. Sci.* **2017**, *10*, 1668–1676. [CrossRef]
27. Bailey, T.P.; Hui, S.; Xie, H.Y.; Olvera, A.; Poudeu, P.F.P.; Tang, X.F.; Uher, C. Enhanced ZT and attempts to chemically stabilize Cu_2Se via Sn doping. *J. Mater. Chem. A* **2016**, *4*, 17225–17235. [CrossRef]
28. Xu, J.; Zhang, W.X.; Yang, Z.H.; Ding, S.X.; Zeng, C.Y.; Chen, L.L.; Wang, Q.; Yang, S.H. Large-scale synthesis of long crystalline $Cu_{2-x}Se$ nanowire bundles by water-evaporation-induced self-assembly and their application in gas sensing. *Adv. Funct. Mater.* **2009**, *19*, 1759–1766. [CrossRef]
29. Ge, Z.H.; Liu, X.Y.; Feng, D.; Lin, J.Y.; He, J.Q. High-performance thermoelectricity in nanostructured earth-abundant copper sulfides bulk materials. *Adv. Energy Mater.* **2016**, *6*. [CrossRef]
30. Jiang, Y.; Wu, Y.; Xie, B.; Zhang, S.Y.; Qian, Y.T. Room temperature preparation of novel $Cu_{2-x}Se$ nanotubes in organic solvent. *Nanotechnology* **2004**, *15*, 283–286. [CrossRef]
31. Poulston, S.; Parlett, P.M.; Stone, P.; Bowker, M. Surface oxidation and reduction of CuO and Cu_2O studied using XPS and XAES. *Surf. Interface Anal.* **1996**, *24*, 811–820. [CrossRef]
32. Teeter, G. X-ray and ultraviolet photoelectron spectroscopy measurements of Cu-doped CdTe(111)-B: Observation of temperature-reversible Cu_xTe precipitation and effect on ionization potential. *J. Appl. Phys.* **2007**, *102*. [CrossRef]
33. Schellenberger, A.; Schlaf, R.; Pettenkofer, C.; Jaegermann, W. XPS and SXPS studies on in-situ prepared Na/InSe insertion compounds. *Solid State Ion.* **1993**, *66*, 307–312. [CrossRef]
34. Yu, J.L.; Zhao, K.P.; Qiu, P.F.; Shi, X.; Chen, L.D. Thermoelectric properties of copper-deficient $Cu_{2-x}Se$ ($0.05 \leq x \leq 0.25$) binary compounds. *Ceram. Int.* **2017**, *43*, 11142–11148. [CrossRef]
35. Xiao, X.; Xie, W.; Tang, X.; Zhang, Q. Phase transition and high temperature thermoelectric properties of copper selenide $Cu_{2-x}Se$ ($0 \leq x \leq 0.25$). *Chin. Phys. B* **2011**, *20*, 087201. [CrossRef]